Ultra-wideband Modelling of Optical Fibre Nonlinearity in Hybrid-amplified Links

Henrique Buglia, Robert I. Killey, and Polina Bayvel

***Abstract*—Ultra-wideband (UWB) transmission using hybrid Raman amplifier technologies is an attractive option to increase the total throughput of a transmission link satisfying the demands for data traffic in optical fibre systems. This amplification technology achieves improved system performance when compared to that obtained with the utilisation of lumped amplifiers only. However, accurate and real-time system performance estimation is required. This paper presents the characteristics of the first analytical model to estimate the performance of the optical system in the presence of hybrid Raman amplifiers and inter-channel stimulated Raman scattering (ISRS). The model accounts for the fibre nonlinear interference (NLI), amplified spontaneous emission (ASE) generated by Raman amplification (RA) and lumped amplification (LA), and transceiver (TRX) noise. It also allows for any RA setup, such as an arbitrary number of forward (FW) and/or backward (BW) pumps, wavelength-dependent fibre parameters, variable modulation formats, per-channel launch powers and channel bandwidths. The model is used to evaluate the performance of a multi-span 18.4 THz transmission system (with 80-km spans) and capacity-maximising hybrid Raman amplifiers are designed based on a particle swarm optimisation (PSO) algorithm, where the semi-analytical nonlinear model was used to achieve real-time optimisation. An extensive theoretical investigation for different systems configurations ranging from short to metro, long-haul and trans-Atlantic links is described, demonstrating the trade-off between the various sources of noise and amplifier technologies.**

***Index Terms*—Ultra-wideband transmission, Raman amplification, lumped amplification, hybrid amplification, S+C+L band transmission, closed-form approximation, Gaussian noise model, nonlinear interference, nonlinear distortion, optical fibre communications, inter-channel stimulated Raman scattering.**

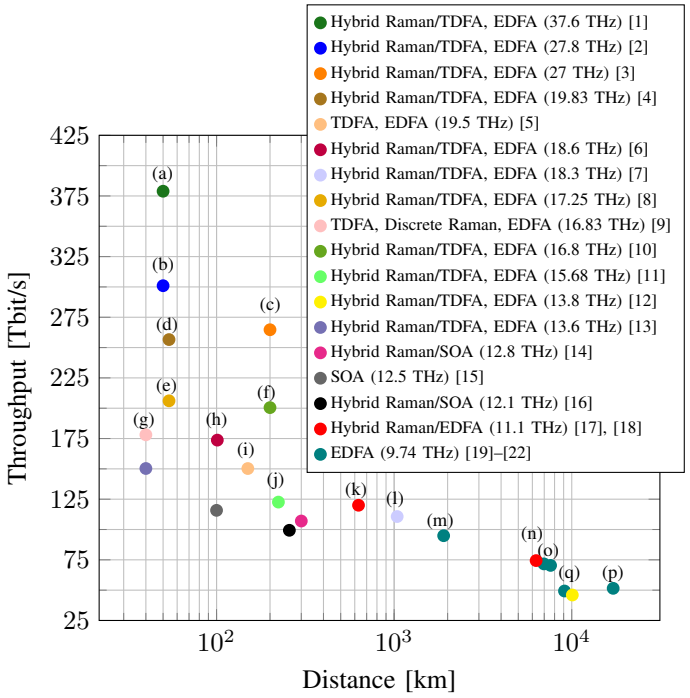

Fig. 1. Record data throughput versus distance for SMF, not including spectral gaps between amplifier gain bandwidths, with the most recent and key results highlighted in the figure: (a) [1], (b) [2], (c) [3], (d) [4], (e) [8], (f) [10], (g) [9], (h) [6], (i) [5], (j) [11], (k) [17], (l) [7], (m) [19], (n) [18], (o) [20], (p) [22] and (q) [12].

I. Introduction

THE exponential growth of bandwidth-hungry internet services including high-definition video streaming, cloud computing, artificial intelligence, Big Data and the Internet of Things have generated the need for new advances in optical data transmission technologies to enable ultra-high throughputs with minimal latencies. Approaches to satisfy growing traffic demand include UWB transmission and space-division multiplexing (SDM) [23]–[26]. For UWB transmission systems, exploring the low-loss wavelength window of a silica-based optical fibre, as shown in Fig. 2, requires the utilisation of new amplifier technologies in addition to erbium-doped fibre amplifiers (EDFA), operating beyond C+L bands. These include thulium-doped fibre amplifiers (TDFA), semiconductor optical amplifiers (SOA) and RA [1]–[18], which have been used over the past few years to achieve milestones of data throughput in single-mode fibres (SMF) over different distances, as shown in Fig. 1 [26].

Almost all recent works, shown as letters (a-q) in Fig. 1, achieved record transmission using a combination of lumped and RA, also known as hybrid-amplification technology. Such a strategy exploits the superior ASE-noise performance of RA when compared to the LA, enabling an increase in the achievable total throughput of the deployed systems [27]. RA can be divided into two types, namely distributed RA and discrete RA. For the former, the pumps are injected into the transmission fibre, while for the latter a separate fibre is used as the amplification stage. In both cases, the pumps interact with the signal to provide the desired signal amplification.

Together with new amplifier technologies, the necessity of maximising the system throughput in optical networks requires the development of real-time models to overcome

This work is funded by the EPSRC studentship EP/T517793/1 and the Microsoft 'Optics for the Cloud' Alliance.

The authors are with the Optical Networks Group, University College London, Department of Electronic and Electrical Engineering, Roberts Building, Torrington Place, London WC1E 7JE, U.K (e-mail: {henrique.buglia.20; r.killey; p.bayvel}@ucl.ac.uk).

This article has been accepted for publication in IEEE/OSA Journal of Lightwave Technology. This is the author's version which has not been fully edited and content may change prior to final publication. Citation information: DOI 10.1109/JLT.2024.3439999

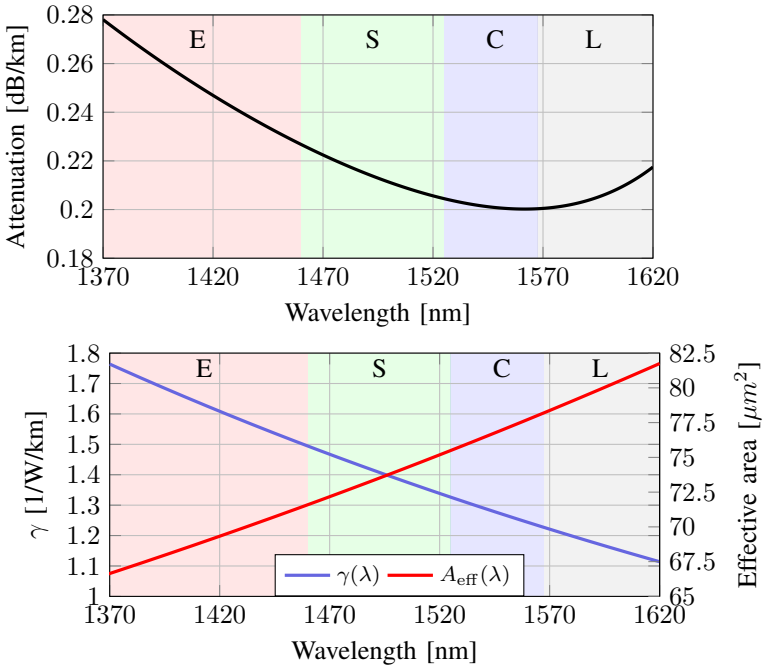

Fig. 2. Wavelength-dependent attenuation coefficient, nonlinear parameter and effective area of an ITU-T G652.D fibre.

the computational complexity of UWB simulations. These models have been developed via closed-form expressions of the Gaussian noise (GN) model and its extensions [28]–[33]. This model offers a simple way of estimating the fibre NLI by treating it as additive GN and numerous closed-form expressions have been proposed to date [34] to speed up the time-consuming computation of the integral expressions involved in it. Of interest for UWB transmission systems are closed-form expressions for the GN model in the presence of the ISRS effect [30], namely ISRS GN model. Closed-form expressions of this model were derived in [35]–[43].

However, most of the aforementioned works were developed for lumped amplifiers, limiting the validity of the models to this amplification scheme. As mentioned, current high-capacity optical fibre systems require nonlinear models capable of accounting also for distributed RA, enabling the assessment of hybrid-amplified optical links. This latter approach enables an increase in the data throughput of deployed optical systems when compared to those employing LA technologies alone. More importantly, these models need to be general and valid for all the RA setups, as the properties of the optical network change depending on the amount of data transmitted, requiring different amplification setups. The works published in [39], [40] enable RA amplification, however, it is limited to FW pumping amplification schemes, and were applied only over C-band systems. The same applies in [44], which is only valid for 2$^{\text{nd}}$ order backward Raman amplification (RA).

The first nonlinear model capable of accurately estimating UWB hybrid-amplified links for any system setup was developed in the works [45]–[48] (recently, another nonlinear closed-form model valid for arbitrary Raman setup was published in [49]). Among the general characteristics of this model, it includes the NLI noise generated by RA together with the ISRS effect, and it offers flexibility, being suitable for any RA setup, such as FW and/or BW pumping amplification schemes, arbitrary-order RA, and arbitrary constellations designs, e.g., Gaussian [46], shaped or square [47] modulation formats. Additionally, the work in [48] includes, for the first time a complete model of ASE noise generated by hybrid amplifiers, consisting of both the ASE noise generated by the Raman and the lumped amplification stages.

This work describes a comprehensive model of hybrid-amplified transmission systems. A detailed characterisation of capacity-maximising hybrid amplifiers is given for different configurations, such as hybrid-FW, hybrid-BW, and hybrid-FW+BW RA. We consider S-, C-, L-band systems, with an optical transmission bandwidth of 18.4 THz (145.7 nm) and we design and model a transmission system using hybrid amplification, where launch power, FW and BW pumps are optimised to achieve the maximum system throughput in a distributed Raman pumping configuration. The NLI and ASE noise contributions are calculated using the models in [46], [48], where the wavelength-dependent nonlinear parameter (γ) and effective core area (A_{eff}) shown in Fig. 2 are included and validated using the integral ISRS GN model [30]. The overall system performance is presented, identifying each source of noise and its contributions to the total SNR, analysing the relation of these noise sources with the capacity-achieving amplifier characteristics. Finally, a comparison of these optimised systems with one optimised to operate over a lumped amplifier scheme is carried out, enabling us to quantify potential increases in throughput through the use of RA schemes.

This paper is structured as follows, Sec II describes the ISRS effect and RA, and how it affects the NLI noise of the system. Sec. III presents the nonlinear model used to compute and estimate all the results of this paper. Sec. IV describes the transmission system setup. Sec V describes the pump and launch power optimisation algorithm used to obtain capacity-achieving hybrid amplifiers. Sec. VI gives the optimised amplifier characterisation in terms of its on-off gain and power profile evolution. Sec. VII presents the contributions to the total noise of each one of the noise sources, the whole system performance based on the overall SNR, and a discussion on the model complexity. Sec. VIII compares the optimised hybrid-amplifier system performance, with that of a system designed and optimised to operate using lumped amplifiers, with conclusions summarised in Sec. IX.

II. Inter-channel Stimulated Raman Scattering and Raman Amplification

This section describes the effects of ISRS and RA, which are jointly included in the closed-form expression derived in [46]. The inclusion of these effects is essential for modelling any UWB system that uses RA technologies.

In the framework of the GN model for UWB systems, the NLI noise is dependent on the injected optical power evolution along the fibre distance. Thus, any nonlinear effect that alters the channel power distribution, will also alter the NLI noise distribution in each channel. This is the case with the ISRS effect and the RA.

This article has been accepted for publication in IEEE/OSA Journal of Lightwave Technology. This is the author's version which has not been fully edited and content may change prior to final publication. Citation information: DOI 10.1109/JLT.2024.3439999

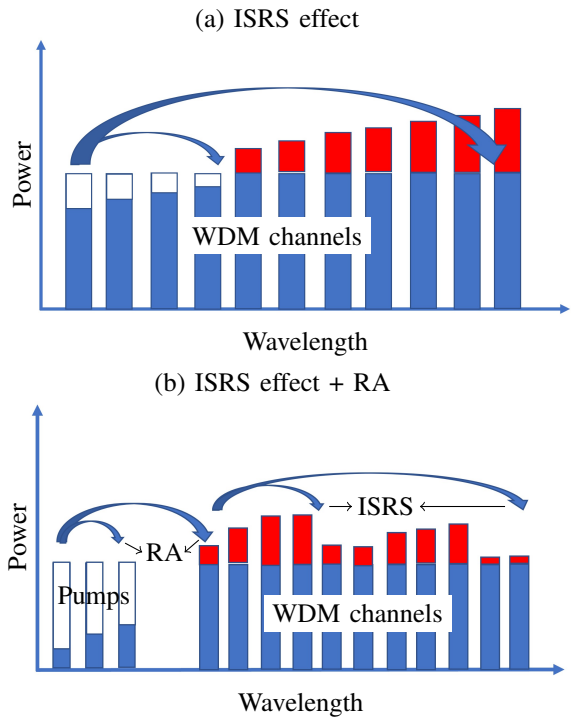

Fig. 3. Illustration of the ISRS effect (a) only and (b) jointly with RA.

Due to the ISRS effect, shorter-wavelength channels transfer power to longer-wavelength channels, as depicted in Fig. 3.(a). This power transfer increases the NLI noise for channels located at longer wavelengths, due to their increased power levels. Similarly, the opposite effect happens for the shorter-wavelength channels. This does not mean that the total NLI is always higher for higher-wavelength channels, as the effect of dispersion and attenuation must also be taken into account in the NLI noise estimation.

The amount of power that is transferred from one channel to another follows the Raman gain spectrum shown in Fig. 4, and it depends on the frequency separation of the channels and the frequency of the channel of interest (COI) f_i, achieving a maximum at around a 13.4 THz frequency separation. For lumped-only amplified systems, closed-form expressions of the GN model were previously derived - with the inclusion of ISRS - in the works [35]–[38], [41]–[43].

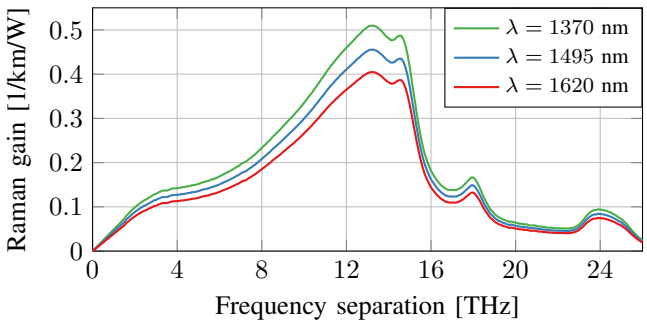

Fig. 4. Raman gain spectrum of an ITU-T G652.D fibre for three different wavelengths.

RA has a similar effect when compared to the ISRS effect. It also produces a power transfer, but from pumps to the channels. When acting jointly with the ISRS effect, this transfer of power occurs in all directions, i.e., from pumps to pumps, pumps to channels and channels to channels, as depicted in Fig. 3.(b). It also follows the Raman gain spectrum in Fig. 4 and in this case, the amount of power transferred from the pumps to each channel will be dependent on the pump wavelengths and their powers. The pumps are usually chosen to give gains in specific portions of the signal spectrum. This selection is done by placing the pumps at an approximate distance of 13.4 THz from the desired regions of the signal spectrum to be amplified.

Due to increased power which is transferred from the pumps to the WDM spectra, the amount of NLI noise present in the signal when compared to the LA case is higher for Raman-amplified links (assuming the same signal launch power for both cases). Despite this disadvantage, Raman-amplified links still generally perform better than LA because of the reduced levels of ASE noise. This is shown in detail in Secs. VII and VIII. For RA systems, closed-form expressions were derived in [39], [40], [44]–[46], [48], [49]. More general cases are covered by the closed-form expressions in [45]–[48], as they are valid for all scenarios of Raman-amplified systems, such as an arbitrary number of FW and/or BW pumps, wavelength-dependent fibre parameters, variable modulation formats, per-channel launch powers and channel bandwidth.

The ISRS effect and RA also affect the optimum launch power distribution and the pump wavelengths and powers which maximise the system throughput. This is because the NLI and ASE noise depend on the per-channel launch power and on the pump wavelength and power allocation. Moreover, this multidimensional-optimisation problem is non-convex [50]. For LA in the presence of ISRS, this fact was discussed and analysed using global optimisation algorithms such as evolutionary algorithms (EA) [51], [52], PSO [24], [25], artificial neural network (ANN) [53] and faster but sub-optimal strategies [54]. Most importantly, the speed of these algorithms has been improved through analytical closed-form expressions [55], [56] or even ANN [57], [58] models that estimate the NLI in the presence of ISRS. For Raman-amplified links, however, this topic has been only explored recently in [40], [48], [59]–[61] due to the very recent development of closed-form expressions fully able to account for all RA setups [45]–[49]. This topic is explored throughout this paper in Sec.V.

III. Nonlinear Model

This section presents the analytical nonlinear model used to derive the results of this paper. Compared to [46], [48], the dependence of γ and A_{eff} on the signal wavelength (see Fig. 2) is included in the closed-form model equations following the approach in [33]. The coupled signal power profile evolution equations are first introduced for each amplification scheme (RA and LA), followed by the equations characterising the ASE and NLI noise.

A. The received SNR

To estimate the total SNR, the impairments arising from the TRX, inline optical amplifiers to compensate for the fibre loss, and fibre nonlinearities are taken into account as additive terms, such that each source of impairment is statistically independent of one another. The received total SNR for the i^{th} WDM channel after the n^{th} amplifier is then given by

$$\begin{aligned}\mathrm{SNR}_i^{-1} &\approx \mathrm{SNR}_{\mathrm{TRX}}^{-1} + \mathrm{SNR}_{\mathrm{ASE}}^{-1} + \mathrm{SNR}_{\mathrm{NLI}}^{-1} = \\ &= \left(\frac{P_i}{\kappa_i P_i + P_{\mathrm{ASE}_i} + \eta_n(f_i) P_i^3}\right)^{-1},\end{aligned} \tag{1}$$

where $\mathrm{SNR}_{\mathrm{TRX}}$, $\mathrm{SNR}_{\mathrm{ASE}}$ and $\mathrm{SNR}_{\mathrm{NLI}}$ are the SNR from the transceiver subsystem (the back-to-back implementation penalty), the ASE from the optical amplifier (RA and/or LA) used to compensate for the fibre loss and the accumulated NLI, respectively. n is the number of spans, i is the COI index, P_i is its launch power, $\kappa_i = 1/\mathrm{SNR}_{\mathrm{TRX}_i}$, P_{ASE_i} is the ASE noise power, and $P_{\mathrm{NLI}_i} = \eta_n(f_i) P_i^3$ is the NLI noise power after n spans. Eq. (1) assumes that the input power is completely recovered after each amplifier. Throughout the remainder of this paper to simplify the analysis, we will consider an ideal TRX, such that $\mathrm{SNR}_{\mathrm{TRX}} \to \infty$. A comprehensive study of the TRX noise impact on the system performance can be found in [25].

B. Signal power profile evolution

Let $\rho(z, f_i) = \frac{P_i(z)}{P_i(0)}$ be the normalised signal power profile evolution along the optical fibre. For distributed Raman amplifiers, the evolution of the COI power along the fibre distance is written as

$$\begin{aligned}\pm\frac{\partial P_i}{\partial z} = &- \sum_{k=i+1}^{\mathrm{N_{ch}}} \frac{f_k}{f_i} g_i(|\Delta f|)(P_k + P_{\mathrm{ASE},k}) P_i - \\ &- \sum_{p:f_i>f_p} \frac{f_p}{f_i} g_i(|\Delta f|)(P_p + P_{ASE,p}) P_i + \\ &+ \sum_{k=1}^{i-1} g_i(|\Delta f|)(P_k + P_{\mathrm{ASE},k}) P_i + \\ &+ \sum_{p:f_i<f_p} g_i(|\Delta f|)(P_p + P_{\mathrm{ASE},p}) P_i - \alpha_i P_i,\end{aligned} \tag{2}$$

where, P_i, f_i are the power and frequency of the COI, P_k, f_k are the power and frequency of the remaining WDM channels, P_p, f_p are the power and the frequency of the pumps, $g_i(|\Delta f|)$ is the wavelength-dependent polarisation averaged, normalized (by the wavelength-dependent $A_{\mathrm{eff},i}$) Raman gain spectrum for a frequency separation $|\Delta f| = |f_i - f_j|$, $j = k, p$ and α_i is the wavelength-dependent attenuation coefficient. $P_{\mathrm{ASE},i}$, $P_{\mathrm{ASE},k}$ and $P_{\mathrm{ASE},p}$ are the ASE noise respectively in the COI, channel k and pump p. The symbol $\pm$ represents the pump under consideration, i.e., $+$ for FW-pump and $-$ for BW-pump configurations. The pump and remaining channel equations are obtained by replacing $i = p, k$ in Eq. (2). Note that, this equation is solved for each span, where the accumulated ASE noise at the end of each span is used as the initial condition for the following span.

In the right-hand side of Eq. (2), the first and third terms represent respectively the COI power loss and gain due to ISRS effect, and the second and fourth terms represent the COI loss and gain due to RA. Usually, pumps are placed on the right-hand side of the WDM frequency spectrum (and not in the middle), such that the second term is zero. Finally, the last term is the COI power loss due to wavelength-dependent fibre attenuation. Note that, both the RA and the ISRS effect are influenced by the ASE noise. The impact of the ASE noise in Eq. (2) is computed in Sec.VII.

In the case of LA, where no pumps are present in the signal spectrum, it is shown to be a good approximation to also neglect the ASE coupled noise and consider only the fibre loss and the ISRS effect, such that, Eq. (2) reduces to

$$\begin{aligned}\frac{\partial P_i}{\partial z} = &- \sum_{k=i+1}^{\mathrm{N_{ch}}} \frac{f_k}{f_i} g_i(|\Delta f|) P_k P_i + \\ &+ \sum_{k=1}^{i-1} g_i(|\Delta f|) P_k P_i - \alpha_i P_i.\end{aligned} \tag{3}$$

C. ASE noise

For Raman-amplified links, the ASE noise power at the frequency of the i^{th} channel, P_{ASE_i}, is calculated as the solution of the following coupled differential equations [48], [62]:

$$\begin{aligned}\frac{\partial P_{ASE,i}}{\partial z} = &- \sum_{k=i+1}^{N_c h} \frac{f_k}{f_i} g_i(|\Delta f|)(P_k + P_{ASE,k})(P_{ASE,i} + 2h\kappa B_i f_i) - \\ &- \sum_{p:f_i>f_p} \frac{f_p}{f_i} g_i(|\Delta f|)(P_p + P_{ASE,p})(P_{ASE,i} + 2h\kappa B_i f_i) + \\ &+ \sum_{k=1}^{i-1} g_i(|\Delta f|)(P_k + P_{ASE,k})(P_{ASE,i} + 2h\kappa B_i f_i) + \\ &+ \sum_{p:f_i<f_p} g_i(|\Delta f|)(P_p + P_{ASE,p})(P_{ASE,i} + 2h\kappa B_i f_i) - \alpha_i P_{ASE,i},\end{aligned} \tag{4}$$

with $\kappa = 1 + \eta = 1/(1 - exp(-h\Delta f/k_B/T))$, where η is the phonon occupancy factor, h is the Planck constant, T is the temperature of the system and k_B is Boltzmann's constant. $P_{ASE,k}$ and $P_{ASE,p}$ are respectively the ASE noise from channel k and the pump p. B_i is the bandwidth of the COI. The ASE equations for the remaining WDM channels and pumps are obtained by setting $i = k$ and $i = p$ respectively. Eq. (4) is solved for each one of the spans with initial conditions at the beginning of the first span as $P_{\mathrm{ASE},i} = P_{\mathrm{ASE},k} = P_{\mathrm{ASE},p} = 0$.

For lumped amplifiers, the ASE noise in channel i after one span, $P'_{\mathrm{ASE},i}$ is approximated by

$$P'_{\mathrm{ASE},i} = 2(G_i - 1) n_{sp,i} h f_i B_i, \tag{5}$$

where $n_{sp,i} \approx \frac{G_i NF - 1}{2(G_i - 1)}$ is the spontaneous emission factor, with NF the amplifier noise figure, and $G_i = P_i(L)/P_i(0)$ is the amplifier gain at the frequency of the i^{th} channel, where $P_i(0)$ and $P_i(L)$ are the powers of channel i at the input and output of the considered span, respectively.

For hybrid-amplified links, the ASE noise generated by distributed Raman amplification, obtained from Eq. (4), is amplified by the ideal lumped amplifier gain (G_i) placed at

the end of the fibre. The total ASE noise is then given by $P''_{\text{ASE},i} = G_i P_{\text{ASE},i} + P'_{\text{ASE},i}$.

D. NLI noise

This section presents the equations used to calculate the NLI noise assuming a Gaussian-modulated signal. An extension of these equations for arbitrary-modulated signals can be found in [47].

For any amplification technique, the NLI noise is given by $P_{\text{NLI},i} = \eta_n(f_i) P_i^3$. The nonlinear coefficient $\eta_n(f_i)$ can be approximated as

$$\eta_n(f_i) \approx \sum_{j=1}^{n} \left[\frac{P_{i,j}}{P_i}\right]^2 \cdot [\eta_{\text{SPM}_j}(f_i) n^{\epsilon} + \eta_{\text{XPM}_j}(f_i)], \tag{6}$$

where $\eta_{\text{SPM}_j}(f_i)$ is the self-phase modulation (SPM) contribution and $\eta_{\text{XPM}_j}(f_i)$ is the total cross-phase modulation (XPM) contribution to the NLI both generated in the j^{th} span. $P_{i,j}$ is the power of channel i launched into the j^{th} span, ϵ is the coherent factor [28, Eq. (22)]. In Eq. (6), the four-wave mixing (FWM) contributions to the NLI are neglected, the SPM is assumed to accumulate coherently along the fibre spans, while the XPM is assumed to accumulate incoherently - the accuracy of these assumptions was validated in [36]. For convenience of notation, the j dependence of the SPM and XPM contribution is suppressed throughout this paper.

The XPM contribution ($\eta_{\text{XPM}}(f_i)$) to the NLI in Eq. (6) is obtained by summing over all COI-interfering pairs present in the transmitted signal, i.e,

$$\eta_{\text{XPM}}(f_i) = \sum_{k=1, k\neq i}^{N_{ch}} \eta_{\text{XPM}}^{(k)}(f_i), \tag{7}$$

where N_{ch} is the number of WDM channels and $\eta_{\text{XPM}}^{(k)}(f_i)$ is the XPM contribution to the NLI of a single interfering channel k on channel i. In Eq. (7), the XPM contributions from the COI-pump pairs are neglected, i.e., $\sum_{p=1}^{N_p} \eta_{\text{XPM}}^{(p)}(f_i) = 0$, where N_{p} is the number of pumps (if any). This was shown to be a reasonable assumption when pumps are far away from the WDM spectra [63].

For Raman-amplified links, semi-analytical expressions for the XPM and SPM NLI contributions of Eq. (6) were previously derived in [46], respectively as

$$\begin{aligned}
\eta_{\text{XPM}}^{(k)}(f_i) = {} & \frac{32}{27}\frac{\gamma_i^2}{B_k}\left(\frac{P_k}{P_i}\right)^2 \sum_{\substack{0\le l_1+l_2\le 1\\ 0\le l'_1+l'_2\le 1}} \Upsilon_k \Upsilon'_k \frac{1}{\phi_{i,k}(\alpha_{l,k}+\alpha'_{l,k})} \times \\
& \times \Bigg\{ 2(\kappa_{f,k}\kappa'_{f,k} + \kappa_{b,k}\kappa'_{b,k}) \left[\operatorname{atan}\left(\frac{\phi_{i,k}B_i}{2\alpha_{l,k}}\right) + \operatorname{atan}\left(\frac{\phi_{i,k}B_i}{2\alpha'_{l,k}}\right)\right] + \\
& + \pi \Bigg[-(\kappa_{f,k}\kappa'_{b,k} + \kappa_{b,k}\kappa'_{f,k}) \left(\operatorname{sign}\left(\frac{\alpha_{l,k}}{\phi_{i,k}}\right) e^{-|\alpha_{l,k}L|} + \right. \\
& + \left. \operatorname{sign}\left(\frac{\alpha'_{l,k}}{\phi_{i,k}}\right) e^{-|\alpha'_{l,k}L|}\right) + (\kappa_{f,k}\kappa'_{b,k} - \kappa_{b,k}\kappa'_{f,k}) \times \\
& \times \left(\operatorname{sign}(-\phi_{i,k})\, e^{-|\alpha_{l,k}L|} + \operatorname{sign}(\phi_{i,k})\, e^{-|\alpha'_{l,k}L|}\right) \Bigg] \Bigg\}
\end{aligned} \tag{8}$$

and

$$\begin{aligned}
\eta_{\text{SPM}}(f_i) = {} & \frac{16}{27}\frac{\gamma_i^2}{B_i^2} \sum_{\substack{0\le l_1+l_2\le 1\\ 0\le l'_1+l'_2\le 1}} \Upsilon_i \Upsilon'_i \frac{\pi}{\phi_i(\alpha_{l,i}+\alpha'_{l,i})} \times \\
& \times \Bigg\{ 2(\kappa_{f,i}\kappa'_{f,i} + \kappa_{b,i}\kappa'_{b,i}) \left[\operatorname{asinh}\left(\frac{3\phi_i B_i^2}{8\pi\alpha_{l,i}}\right) + \operatorname{asinh}\left(\frac{3\phi_i B_i^2}{8\pi\alpha'_{l,i}}\right)\right] + \\
& + 4\ln\left(\sqrt{\frac{\phi_i L}{2\pi}} B_i\right) \Bigg[-(\kappa_{f,i}\kappa'_{b,i} + \kappa_{b,i}\kappa'_{f,i}) \left(\operatorname{sign}\left(\frac{\alpha_{l,i}}{\phi_i}\right) e^{-|\alpha_{l,i}L|} + \right. \\
& + \left. \operatorname{sign}\left(\frac{\alpha'_{l,i}}{\phi_i}\right) e^{-|\alpha'_{l,i}L|}\right) + (\kappa_{f,i}\kappa'_{b,i} - \kappa_{b,i}\kappa'_{f,i}) \times \\
& \times \left(\operatorname{sign}(-\phi_i)\, e^{-|\alpha_{l,i}L|} \operatorname{sign}(\phi_i)\, e^{-|\alpha'_{l,i}L|}\right) \Bigg] \Bigg\},
\end{aligned} \tag{9}$$

where

$$\begin{aligned}
\phi_i &= -4\pi^2 \left(\beta_2 + 2\pi\beta_3 f_i\right), \\
\phi_{i,k} &= -4\pi^2 \left(f_k - f_i\right)\left[\beta_2 + \pi\beta_3 \left(f_i + f_k\right)\right],
\end{aligned}$$

$$\begin{aligned}
T_{f,i} &= -\frac{P_f C_{f,i}(f_i - \hat{f})}{\alpha_{f,i}}, & T_i &= 1 + T_{f,i} - T_{b,i} e^{-\alpha_{b,i}L}, \\
T_{b,i} &= -\frac{P_b C_{b,i}(f_i - \hat{f})}{\alpha_{b,i}}, & \alpha_{l,i} &= \alpha_i + l_1\alpha_{f,i} - l_2\alpha_{b,i}, \\
& & \kappa_{f,i} &= e^{-(\alpha_i + l_1\alpha_{f,i})L}, \\
& & \kappa_{b,i} &= e^{-l_2\alpha_{b,i}L},
\end{aligned}$$

$$\Upsilon_i = T_i \left(\frac{-T_{f,i}}{T_i}\right)^{l_1} \left(\frac{T_{b,i}}{T_i}\right)^{l_2},$$

β_2 is the group velocity dispersion (GVD) parameter, β_3 is the linear slope of the GVD parameter and B_k is the bandwidth of the channel k. The coefficients Υ'_i, $\alpha'_{l,i}$, $\kappa'_{f,i}$ and $\kappa'_{b,i}$ are respectively the same ones as Υ_i, $\alpha_{l,i}$, $\kappa_{f,i}$ and $\kappa_{b,i}$ but with the indices l_1 and l_2 replaced by l'_1 and l'_2. L is the fibre length, P_f is the sum of the channel together with the FW pump powers and P_b is the sum of the BW pump powers. $\hat{f}$ is the average frequency of the pumps. α_i, $\alpha_{f,i}$ and $\alpha_{b,i}$ are fibre attenuation coefficients, $C_{f,i}$ and $C_{b,i}$ is the slope of a linear regression of the normalised Raman gain spectrum.

The determination of the channel-dependent coefficients α_i, $\alpha_{f,i}$, $\alpha_{b,i}$, $C_{f,i}$ and $C_{b,i}$ follows the strategy described in [46], i.e, the following semi-analytical function is used:

$$\rho(z, f_i) = e^{-\alpha_i z}[1 - (C_{f,i} P_f L_{\text{eff}} + C_{b,i} P_b \tilde{L}_{\text{eff}})(f_i - \hat{f})], \tag{10}$$

where

$$\begin{aligned}
L_{\text{eff}}(z) &= (1 - e^{-\alpha_{f,i} z})/\alpha_{f,i} \quad , \\
\tilde{L}_{\text{eff}}(z) &= (e^{-\alpha_{b,i}(L-z)} - e^{-\alpha_{b,i}L})/\alpha_{b,i} \quad .
\end{aligned}$$

The coefficients α_i, $\alpha_{f,i}$, $\alpha_{b,i}$, $C_{f,i}$ and $C_{b,i}$ are then optimised using optimisation routines (e.g, nonlinear least-squares fitting), such that the values obtained for the 5 coefficients in Eq. (10), correctly reproduce the power profile obtained from the Raman differential equations in the presence of RA, i.e, from Eq. (2).

The parameters α_i, $C_{f,i}$, $C_{b,i}$, $\alpha_{f,i}$, and $\alpha_{b,i}$ can be interpreted as modelling respectively the fibre loss, the gain/loss

due to FW-RA and BW-RA together with ISRS and how fast the channel gain/loss due to the FW-RA and BW-RA together with ISRS extinguish along the fibre. This fitting optimisation procedure enables the utilisation of Eqs. (8) and Eq. (9) in any simulation scenarios, such as any number of pumps, launch power profiles and channel bandwidths. The accuracy of the fitting optimisation step was previously validated in Fig. 3 of [46]. Additionally, the formula is also valid for links made of different span setups - in that case, all the fibre parameters and per-channel launch power depend not only on the channel i but also on the span j. For LA, more simplified equations other than Eqs. (8) and (9) for the SPM and XPM NLI contributions can be used. These equations were published in [36] as Eqs. (10) and (11).

IV. Transmission System Setup

This section describes the transmission system used for all the analyses in this paper. It consists of a WDM signal with N_{ch}=185 channels spaced by 100 GHz and centred at 1539 nm. Each channel is modulated at the symbol rate of 96 GBd, resulting in a total bandwidth of 18.4 THz (145.7 nm), ranging from 1470 nm to 1615 nm, corresponding to transmission over the S- (1470 nm - 1520 nm), C- (1530 nm - 1565 nm) and L- (1570 nm - 1615 nm) bands respectively with 6.7 THz, 4.4 THz, and 5.3 THz each. Spectral gaps of 10 nm and 5 nm are considered, respectively between the S/C and C/L band. The NF of each lumped amplifier placed at the end of each span is assumed to be uniform per band with values of 6 dB, 5 dB, and 6 dB in the S-, C- and L- band, respectively. For simplicity, we consider Gaussian constellations, such that we can directly apply the model in Sec. III, however, other types of constellations could be easily considered by using the additional NLI correction term in [47].

A generic SMF corresponding to an ITU-T G652.D fibre with attenuation, γ and A_{eff} profiles shown in Fig. 2 is considered. The Raman gain spectrum is shown in Fig. 4; this spectrum is normalised for each channel i by the corresponding $A_{\text{eff},i}$ shown in Fig. 2. The dispersion, and dispersion slope, are assumed to be $D = 16.5$ ps nm^{-1}km^{-1} and $S = 0.09$ ps nm^{-2}km^{-1}, respectively.

A transmission link made of multiple spans of 80 km is studied. Simulations were carried out for 1, 10 and 100 spans to simulate distances ranging from short to metro, long-haul and trans-oceanic. A hybrid amplification scheme made of a distributed Raman amplifier followed by an LA is considered. The LA at the end of each span is assumed to be ideal, such that the transmitted power is completely recovered at the end of each span. To that end, after distributed RA, the lumped gain at the end of each span is assumed to be controlled to the target value by using adaptive spectral equalisation and amplifier dynamic gain control devices. A spectrally-uniform launch power profile is considered, which is optimised together with the pumps to maximise the system throughput (see Sec. V). A per-channel launch power profile could also be considered as in [60], however, for simplicity and computational time reduction, we chose to operate with a spectrally uniform one as explained in Sec. V.

V. Throughput Maximisation for Hybrid-Amplified Transmission

This section describes the throughput maximisation strategy used in this paper to maximise the system performance given by Eq. (1). Due to the RA and the ISRS effect, the relation between system performance, pumps' powers and launch power is nonlinear, leading to a $N_{\text{ch}} + N_{\text{p}}$-dimensional non-convex optimisation problem [50]. To solve this problem, numerical optimisation algorithms are required.

The goal of this optimisation is to find the optimum pump wavelengths and powers together with the optimum channel launch power, which maximises the total throughput for the hybrid RA transmission system considered in Sec. IV. The total throughput is bounded above by the AWGN channel capacity:

$$C_{\text{Total}} = \sum_{i=1}^{N_{\text{ch}}} C_i = \sum_{i=1}^{N_{\text{ch}}} 2 \cdot \log_2(1 + \text{SNR}_i), \qquad (11)$$

where SNR_i is obtained from Eq. (1) and C_i is the AWGN capacity for the i^{th} channel. Eq. (11) is the cost function considered in the optimisation, where SNR_i is calculated from Eq. (1). Note that the ASE generated by the distributed Raman stage and by the lumped amplifier are calculated using Eqs. (4) and (5), respectively.

The numerical optimisation algorithm chosen to find a local maximum of (11) is the PSO [64]. The PSO is efficient in exploring the $N_{\text{ch}} + N_{\text{p}}$-dimensional space leading to the surroundings of a good local optimal solution. For this algorithm, we use the Matlab PSO function provided by the global optimisation toolbox. To reduce the complexity of this algorithm, we chose to optimise a spectrally uniform launch power profile, such that each channel carries the same launch power. This enables the reduction of the optimisation space from $N_{\text{ch}} + N_{\text{p}}$ to $N_{\text{p}} + 1$. Moreover, compared to a per-channel launch power optimisation, the penalty in performance by making this assumption is small as shown in [60].

For this optimisation, transmission over a single span is considered, and the solution of this optimisation is used for pumping all the remaining amplifiers in the multi-span transmission scenarios (see Sec. IV). This approach is not optimum as the optimum amplifier design changes slightly for each span. This is because the NLI and the ASE noises generated in each span accumulate in a nonlinear manner. However, this non-optimal choice reduces the complexity of the optimisation algorithm as Eqs. (2) and (4) are solved for a single span only.

We consider three different hybrid-amplification simulation scenarios, each one using the following distributed setup: FW-RA, BW-RA and FW+BW-RA. Over the E- band (1370 nm-1460 nm) we place 8 FW/BW pumps and let the algorithm find the best wavelength and power allocation for these pumps, i.e., the allocation which maximises Eq. (11), considering an ideal lumped amplifier at end of the span to give the remaining signal gain to completely recover the transmitted power. The highest-wavelength pump was chosen to be 10 nm away from the lowest-wavelength channel, such that we can neglect the

TABLE I
PUMPS' POWER AND WAVELENGTH ALLOCATION WHICH YIELDS THE POWER PROFILES SHOWN IN FIG 5.

Forward Raman Pump Scenario							
Wavelength [nm]	1370	1370.3	1411	-	-	-	-
FW pumps' power at $z = 0$ [mW]	249.28	250	250	-	-	-	-
Backward Raman Pump Scenario							
Wavelength [nm]	1370	1412.4	1414.7	1423.9	1452.1	-	-
BW pumps' power at $z = L$ [mW]	249.97	249.86	226.43	46.19	73.21	-	-
BW pumps' power at $z = 0$ [mW]	0.03	0.64	0.67	0.29	2.17	-	-
Forward + Backward Raman Pump Scenario							
Wavelength [nm]	1370.4	1395.6	1402.6	1418.1	1423	1451.2	1460
FW pump power at $z = 0$ [mW]	244.28	164.73	-	-	-	-	-
BW pumps' power at $z = L$ [mW]	-	-	194.6	228	200.28	15.93	133.63
BW pumps' power at $z = 0$ [mW]	-	-	0.15	0.90	1.22	0.87	14.97

XPM-induced products from pumps falling into the WDM spectrum [63].

For the FW-RA and BW-RA, 17 variables are then optimised, of which 1 variable is the spectrally uniform launch power, 8 are the pump powers (FW or BW) and 8 are their respective wavelengths. For the FW+BW-RA, 33 variables are optimised, of which 1 variable is the spectrally uniform launch power, 16 are the pump powers (FW + BW) and 16 are their respective wavelengths. For the PSO algorithm, the number of particles is chosen to be 50 with a maximum of 50 iterations as the stopping criteria. For the algorithm bounds, we let the total channel launch power vary between 10 dBm and 25 dBm, and the power of each pump at the beginning of the fibre vary from 0 mW to 250 mW. At the end of the optimisation, we set 0 power for all the pumps with negligible power at the beginning of the fibre for the FW case, and at the end of the fibre for BW case. For each one of the scenarios considered, the pumps' allocation with non-negligible power found by the described algorithm is shown in Table I. For the FW-RA case, an optimum input launch power per channel of -0.97 dBm was found, resulting in a total launch power of 21.23 dBm, yielding a total throughput of 296.48 Tbit/s. For the BW-RA case, an optimum input launch power per channel of 0.28 dBm was found, resulting in a total launch power of 22.48 dBm and yielding a total throughput of 310.72 Tbit/s. For the FW+BW-RA case, an optimum input launch power per channel of -1.39 dBm was found, resulting in a total launch power of 20.81 dBm and yielding a total throughput of 319.72 Tbit/s. These values are discussed and analysed in detail in the next sections.

Finally, note that the optimisation carried out in this section, may not necessarily be the optimum one, as more pumps could be considered at more wavelengths, increasing the degrees of freedom. Together with this, the optimisation bounds, chosen algorithm and algorithm setup could be changed to achieve better results. The described setup was chosen to achieve fast computational time for the PSO algorithm without requiring the utilisation of GPUs.

VI. HYBRID-AMPLIFIER CHARACTERISATION

This section presents the characterisation of the hybrid amplifier. To that end, for both the optimised scenarios described in Sec. V, we give the power profile evolution along the fibre distance, the hybrid amplifier gain, i.e., the distributed Raman on-off gain followed by the gain provided by the lumped amplifier placed at the end of the span. The results are shown for transmission after 1 span.

The pumps' allocation in terms of wavelengths and powers is shown in Table I for each optimised scenario described in Sec. V. For the FW-RA case, the wavelengths of the pump amplify mostly the S-band signal. For the BW-RA and FW+BW-RA cases, the obtained pump wavelengths can amplify both S- and C- band channels and the shorter channels of the L-band. For all the cases, the longer L-band channels are mainly amplified by the lumped amplifier as the longer possible E-band pump wavelength (1460 nm) is 110 nm (14.4 THz) away from the shorter L-band channel (1570 nm), and thus beyond the peak of the Raman gain spectrum which happens at 13.4 THz (see Fig. 4). Note that the number of pumps obtained in Table 1 depends on the total power allowed for each pump and on the total system losses. In this work, the only source of loss considered is the fibre loss, however in deployed systems, more pumps may be expected due to additional fibre, component and equipment losses.

For the three scenarios described in Sec. V, the per-channel power profile along the distance, i.e., the solution of Eq. (2), are shown in Fig. 5 for (a) FW-RA, (b) BW-RA and (c) FW+BW-RA. Note that, as shown in Eqs. (2) and (4), the intensity of ASE noise generated due to the RA, i.e. ASE noise before LA, is proportional to the intensity of the received launch power profiles. Taking the FW-only and BW-only scenarios as examples, this means that for the FW-RA amplification, low levels of ASE noise before LA are expected and higher NLI noise is generated given the higher power levels propagating along the length of the fibre. In the case of BW-RA, the opposite effect occurs: higher ASE noise before LA is expected and lower NLI noise is produced given the reduced power levels propagating along the fibre distance. However, the generated ASE noise before LA is still amplified by the lumped amplifier placed at the end of the span. These effects are quantified in detail in Sec. VII.

Fig. 5 shows the amplifier gain for hybrid (a) FW-RA, (b) BW-RA and (c) FW+BW-RA. The gains are shown for the optimised distributed Raman amplifier (red) and the lumped amplifier (blue) placed at the end of each span. The total gain, i.e., the sum of the gain from the distributed Raman

This article has been accepted for publication in IEEE/OSA Journal of Lightwave Technology. This is the author's version which has not been fully edited and content may change prior to final publication. Citation information: DOI 10.1109/JLT.2024.3439999

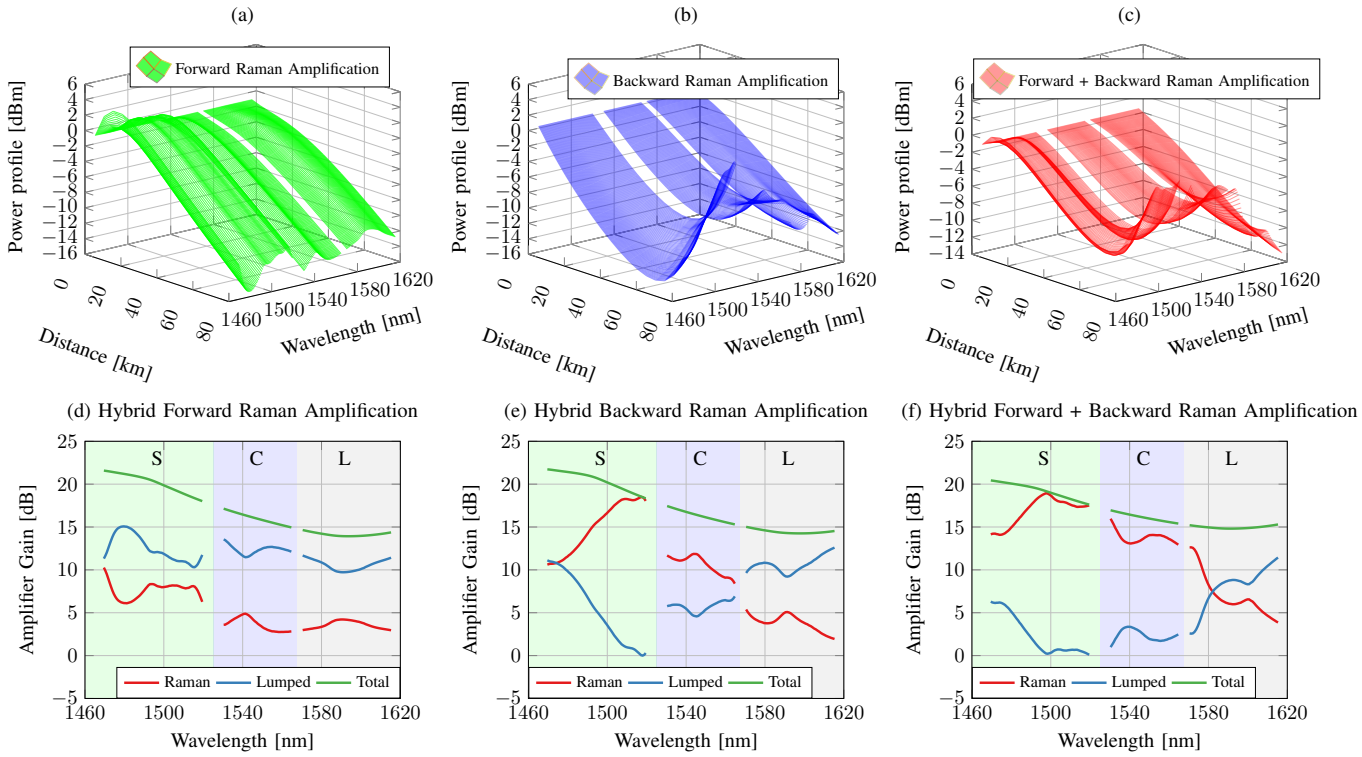

Fig. 5. Top row: per-channel launch power evolution along the fibre distance after 1 span for (a) FW-RA, (b) BW-RA and (c) FW+BW-RA. Bottom row: hybrid amplifier gain after 1 span designed in Sec. V for (d) FW-RA, (e) BW-RA and (f) FW+BW-RA. The gains for each one of the amplification stages are shown in red (RA stage) and blue (LA stage); the total gain is shown in green.

and lumped amplifier stages is also shown in green. For the systems with BW pumps, most of the optimised amplifier gain in the S- and C-bands arises from the distributed Raman stage. L-band channels are far from the pumps and thus do not benefit significantly from the gains in this stage. For FW-RA, most gains come from the LA stage given the high NLI due to the high power levels propagating through the fibre. More interesting is the fact that a full Raman gain in the S- and C-band, with no lumped amplifiers, might not be the best option, as, despite the greater performance of Raman amplifiers in terms of ASE generation, it may massively increase the NLI and ASE noise as a result of high pump powers.

Note that, the total gain (green), or effective fibre loss (standard loss + ISRS effect) is different for each scenario - this is because each one of the systems has different values of total launch power (which changes the intensity of the ISRS effect); indeed for the hybrid FW-RA case, the total optimised power is 21.23 dBm, while these values for the hybrid BW-RA and FW+BW-RA cases are respectively 22.48 dBm and 20.81 dBm.

Because the signal profile evolution along the fibre distance depends on the ASE noise (see Eqs. (2) and (4)), its evolution changes slightly in each span, resulting in different Raman and ideal lumped gains depending on the span under consideration. This effect is well known [65], and is referred to as the droop effect [66], [67]. To analyse this effect, Fig. 6 shows the ideal gain from the lumped amplifier placed at the end of the 1st, 10th and 100th span for the optimised hybrid BW-RA designed in Sec. V. The ideal lumped gain slightly reduces after each span to maintain the correct input/output power. This change is approximately 0.1 dB after 10 spans and 1.2 dB after 100 spans. This effect is negligible for few spans, but relevant for trans-oceanic links. In this work, we use Eq. (2) in its original form, i.e., considering the coupled ASE noise with the signal and thus the droop effect, where the ideal lumped gain is adjusted in each span to recover the transmitted power correctly.

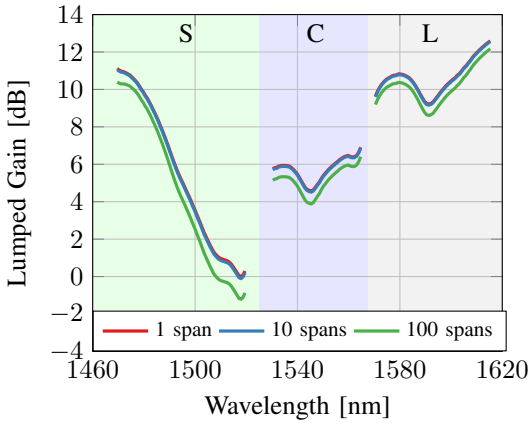

Fig. 6. Ideal gain from the lumped amplifiers placed at the end of the 1st, 10th and 100th span for the optimised hybrid BW-RA scenario.

This article has been accepted for publication in IEEE/OSA Journal of Lightwave Technology. This is the author's version which has not been fully edited and content may change prior to final publication. Citation information: DOI 10.1109/JLT.2024.3439999

VII. System Performance for Hybrid-Amplified Transmission

This section shows the performance of the transmission systems considered in Secs. IV and V, for the three optimised hybrid-amplified systems. The noise sources, namely, ASE from the Raman amplifier, ASE from the lumped amplifier and NLI from the fibre transmission, are separated and analysed for a single span. The total system performance in terms of ASE, NLI and total SNR are then computed for 1, 10 and 100-span transmissions and a detailed discussion of the results is presented. Furthermore, the accuracy of the NLI SNR levels estimated using the model in Sec. III are verified for all the scenarios presented in this section using the integral ISRS GN model [30]. To that end, the wavelength dependence of γ and A_{eff} were also included in this model.

We start by separating and showing each one of the noise sources in Eq. (1). This is demonstrated in Fig. 7 after 1 span transmission. The choice of showing it for 1 span is based on the fact that this is the only scenario where we can separate the ASE noise generated from the Raman amplifier from that generated by LA. This is because after the first span, the total ASE noise (Raman + lumped) is used as the initial condition in Eq. (4), and thus, from the second span onwards, noise from both sources are coupled in the transmission and cannot be separated.

Fig. 7 shows the different noise contributions from Eq. (1), for the three hybrid amplifier schemes. The Raman ASE noise is shown before LA (red) and after being amplified by the ideal lumped amplified (blue) placed at the end of the span. The ASE noise from LA (green) obtained from Eq. (5) is also shown. The amplified Raman and the lumped ASE noise contributions are then summed and shown as the total ASE (purple). Finally, the NLI noise (orange), and the sum of the total ASE and NLI noises are shown as the total noise (brown). For (a) hybrid FW-RA, the NLI noise is higher in portions of the S-band, because most of the Raman amplification happens in this spectral region. On the other hand, for (b) hybrid BW-RA, the ASE noise is the most impactful contribution while the NLI noise has a smaller contribution in the full spectral region. For (c) hybrid FW+BW-RA, the ASE and NLI contributions in the S-band are more balanced and the total noise power levels are limited by both ASE and NLI contributions; in the C- and L-band the system is more impacted by the ASE noise. The explanation for these levels relies on the amount of power and ASE generated along the fibre transmission for each scenario (see Fig. 5 and Sec. VI for a detailed explanation).

Fig. 8 shows the different SNR contributions as a function of wavelength for the transmissions over 1, 10 and 100 spans for (a) FW-RA, (b) BW-RA and (c) FW+BW-RA. The ASE contribution corresponds to the total ASE noise generated by RA and LA.

It is interesting to note the correlation of the SNR profile with the power profiles shown in Fig. 5. Indeed, for the hybrid FW-RA case, shown in Fig. 8(a), the high-power levels at the short wavelengths (see Fig. 5(a)) increases the NLI noise, reducing the SNR, and degrading the performance of those channels; on the other hand, the performance of long-

(a) Hybrid Forward Raman Amplification

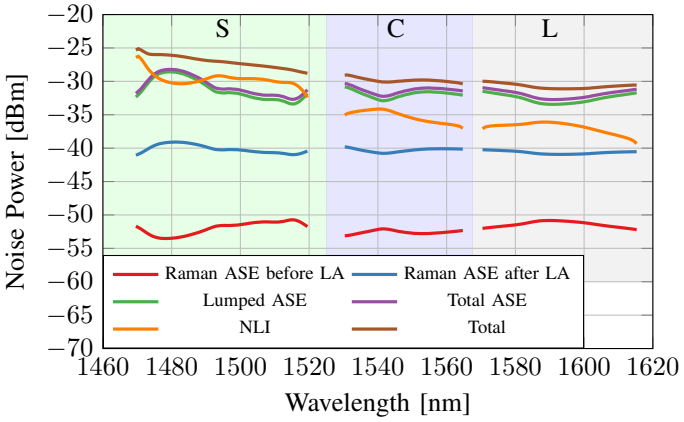

(b) Hybrid Backward Raman Amplification

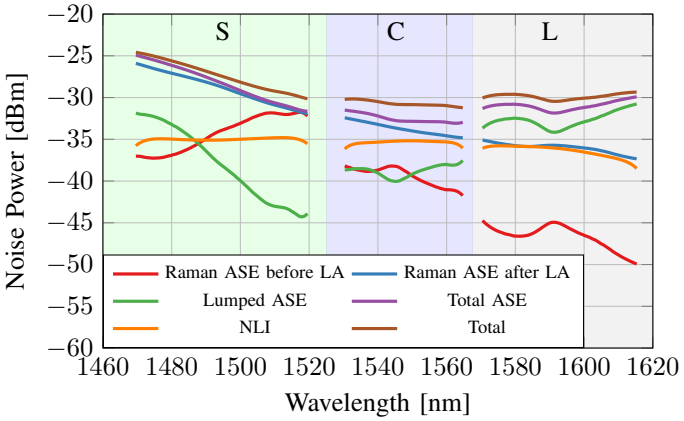

(c) Hybrid Forward + Backward Raman Amplification

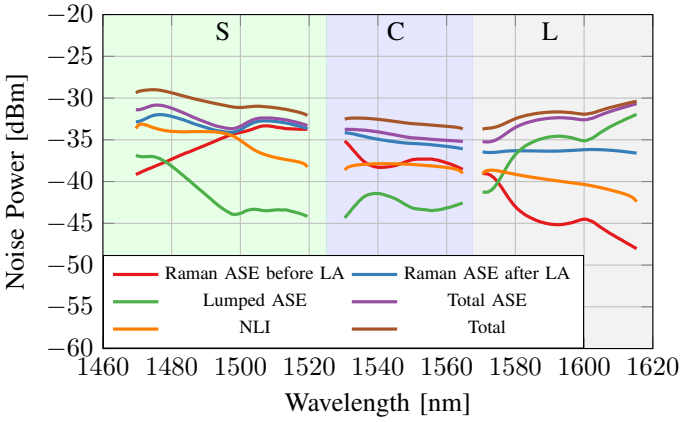

Fig. 7. Noise power contributions after the first span for hybrid (a) FW-RA, (b) BW-RA and (c) FW+BW-RA.

wavelength channels is higher, due to their reduced power levels, yielding to a tilt in the SNR profile. For the hybrid BW-RA case, shown in Fig. 8(b) the increased received power levels at the short wavelengths (see Fig. 5(b)) increases the ASE noise generated by the Raman stage, reducing the SNR and degrading the performance of those channels; on the other hand, the balanced ASE generated from the Raman stage together with the lumped stage increases the performance of the C-band. Almost no Raman gain is obtained in the L-band,

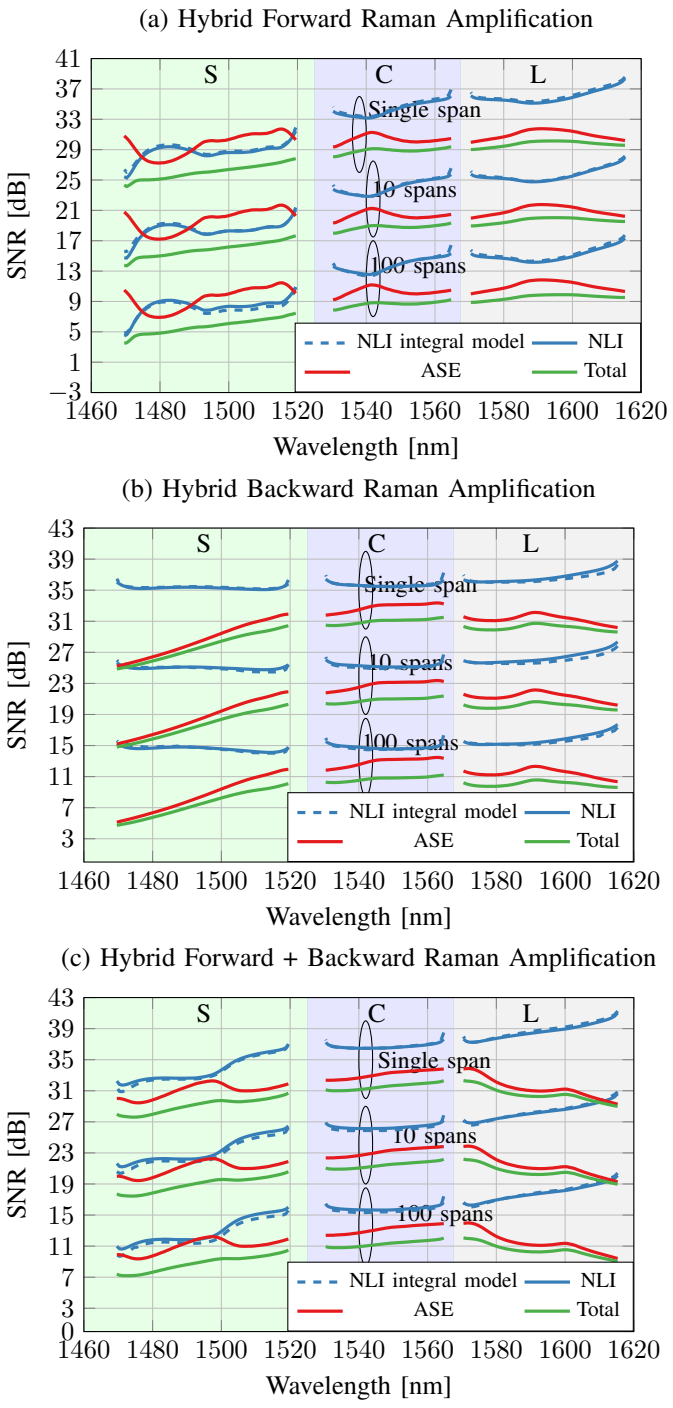

Fig. 8. SNR contributions after the 1st, 10th and 100th span for hybrid (a) FW-RA, (b) BW-RA and (c) FW+BW-RA.

worsening the SNR of these channels because most of the ASE noise is generated by the lumped stage. For the hybrid FW+BW-RA case, shown in Fig. 8(c) the increased power levels at the short wavelengths (see Fig. 5(c)) increase the ASE and NLI noises, reducing the SNR degrading the performance of those channels and yielding a similar SNR curve shape as in the previous case.

NLI SNR estimation using the model in Sec. III and the integral ISRS GN model [30] are shown as blue curves in

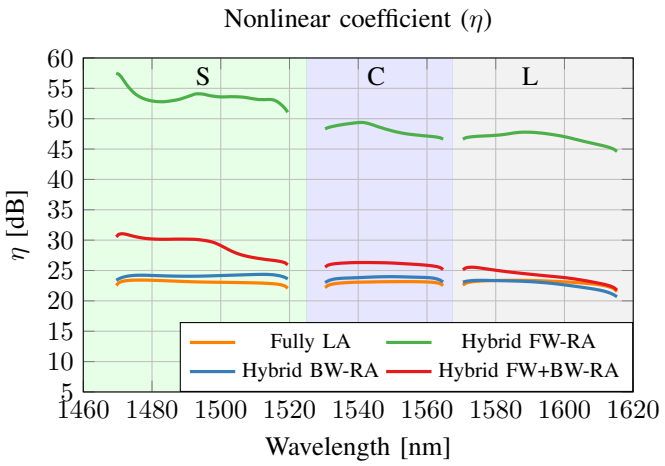

Fig. 9. Nonlinear coefficient after 1 span for the transmission system in Sec. IV for each amplification scheme.

Fig. 8 for accuracy verification. For (a) hybrid FW-RA and (b) hybrid BW-RA, the maximum per-channel error between these models is 1.11 dB and 1.03 dB respectively occurring for the channel located at 1546.7 nm. For (c) hybrid FW+BW-RA, this value is 1.10 dB for the channel located at 1469.6 nm. In each scenario, the maximum per-channel errors occur for the transmission over 100 spans. Furthermore, across all scenarios, the maximum average error is 0.33 dB and occurs for the transmission over 100 spans using hybrid FW+BW-RA.

Regarding a rough estimation of the model complexity, using a standard central processing unit (CPU) without any code parallelisation, one realisation of the closed-form expression in Sec III for all scenarios took less than 5 seconds, with the majority of the time being spent in the fitting optimisation routine which involves fitting Eq. (10) to the power profile obtained by numerically solving Eq. (2). The computation time, however, can be reduced to milliseconds by clever implementation of the fitting optimisation routine, code parallelisation and utilisation of GPUs, as the fitting can be calculated independently for each channel.

VIII. Comparison with Fully Lumped Amplification

This section compares the transmission system described in Secs. IV and V with a fully lumped amplified link, i.e., without any pumps in the transmission fibre, such that the transmitted power is completely recovered with the ideal lumped amplifier placed at the end of each span. To simulate this transmission, the NLI model published in [55] was used with the same transmission setup described in Sec. IV. Note that the wavelength dependence of γ and A_{eff} was also included in this model. The results, in terms of performance, are then compared with those of Sec. VII and the differences are highlighted and discussed in detail.

The first step for carrying out this simulation was to consider a fully lumped transmission system with the same parameters as described in Sec IV. As no pumps are placed in the transmission, we optimised only the total launch power of the system, which resulted in a total optimal launch power of 23.5 dBm, corresponding to 1.3 dBm per channel. This

This article has been accepted for publication in IEEE/OSA Journal of Lightwave Technology. This is the author's version which has not been fully edited and content may change prior to final publication. Citation information: DOI 10.1109/JLT.2024.3439999

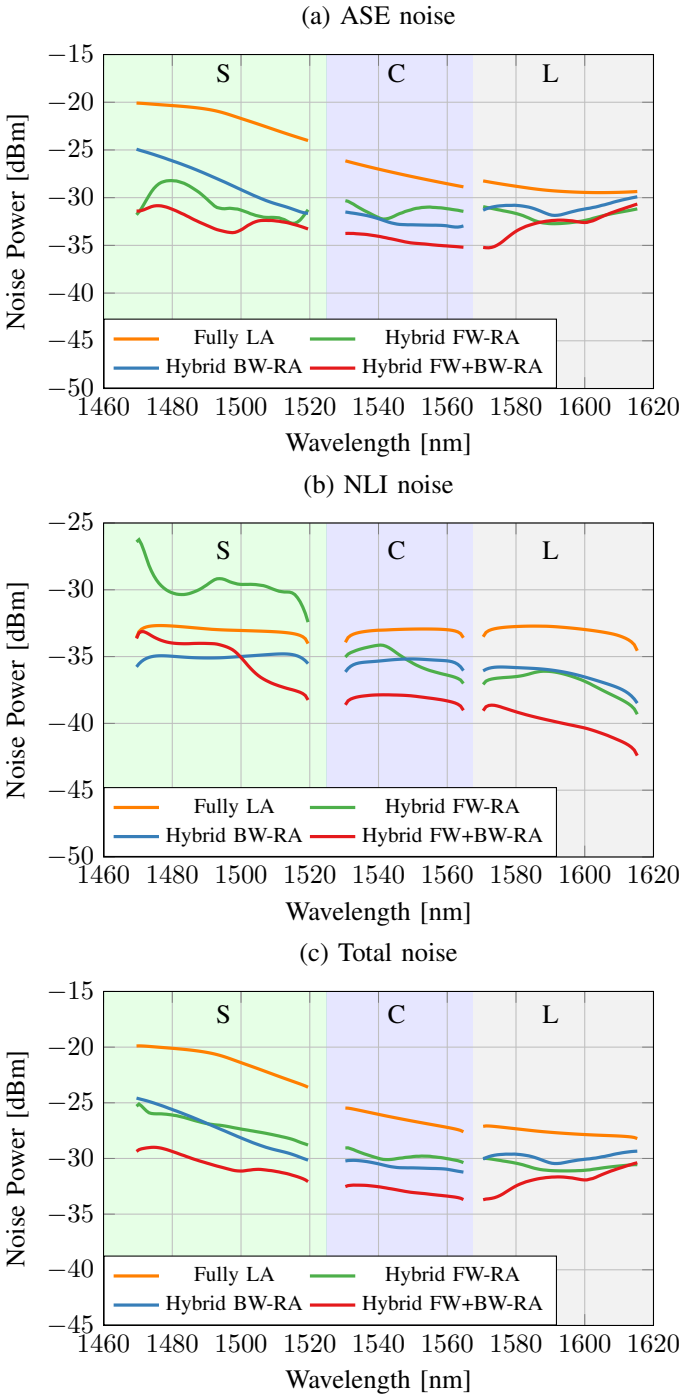

Fig. 10. Different noise power contributions after the 1st span for each amplification scheme.

optimisation resulted in a total throughput of 275.29 Tbit/s over a single-span transmission.

Fig. 9 shows the nonlinear coefficient η (see Eq. (1)) obtained from each one of the amplification schemes, namely, hybrid FW-RA, hybrid BW-RA, hybrid FW+BW-RA and fully LA. The motivation for plotting η is to provide a rough estimate the amount of NLI noise generated by each amplification scheme if the launch power was the same for the optimised amplification schemes considered (this is because η

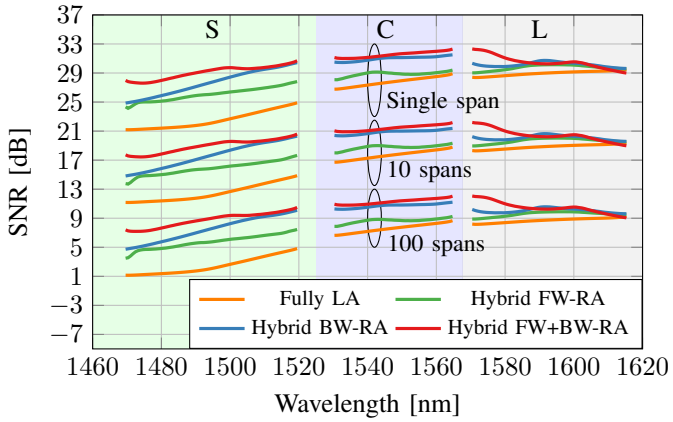

Fig. 11. Total SNR contribution after the 1st, 10th and 100th span for each amplification scheme.

only depends on the normalised launch power profile, and not on its absolute value). This figure shows that the hybrid FW-RA generates higher amounts of NLI noise, because of its increased values of power propagating along the fibre length (see Fig 5), while the LA case generates lower amounts of NLI noise (for the same launch power) because the power is just attenuated by the fibre loss and changed by the ISRS effect, i.e, no pumps are adding additional power in the fibre. Note that, in reality for the systems designed in this paper, because the launch power is different for each amplification scheme and the NLI noise is proportional to this quantity to the power cube ($P_{\text{NLI}} \propto P_i^3$), the absolute amount of NLI noise generated by each scheme depends on the launch power. Indeed, the higher launch power for the fully LA scenario (23.5 dBm) makes this case perform worse than BW-RA and BW+FW-RA cases in terms of NLI noise generation as shown in Fig. 10.(b).

Fig. 10 shows the different noise contributions for each one of the amplification schemes designed in this work. Fig. 10.(a) shows that the LA case presents higher ASE noise generation, which motivates the utilisation of hybrid amplifiers to achieve higher throughput. Fig. 10.(b), shows that the increased total launch power of the LA case (23.5 dBm) generates high amounts of NLI noise. Finally, Fig. 10.(c), shows that, overall, LA is the worst-case scenario in terms of noise generation, followed by the hybrid amplification schemes. However, this is not a complete indication of which amplification scheme is better as the SNR calculation also depends on the launch power.

In order to assess which amplification scheme is best, Fig.11 shows the total SNR contributions for the transmission over 1, 10 and 100 spans for each one of the designed amplifiers. This figure shows that the hybrid FW+BW-RA presents the best compromise between launch power, ASE and NLI noise, achieving the best performance. The worst performance is obtained by the fully lumped case, which is mainly because of its reduced ASE performance. In this figure, the NLI SNR contribution to the total SNR for the lumped case was also validated using the integral model [30], however, results are not shown in this figure. The maximum per-channel error obtained was 0.76 dB at the channel located at 1612.7 nm

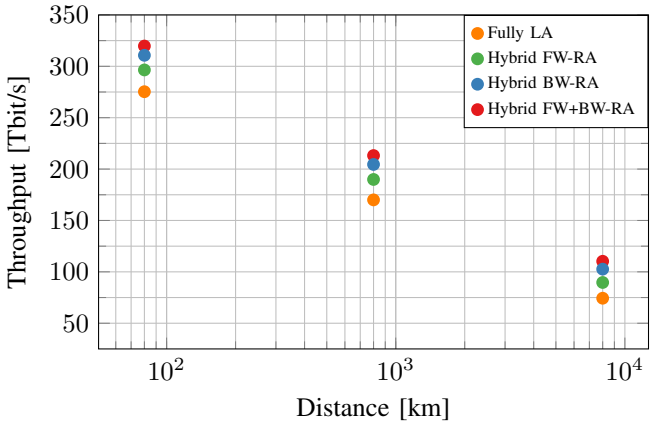

Fig. 12. Total throughput achieved by the different amplification schemes after 1, 10 and 100 spans.

for transmission over 100 spans. The maximum average error obtained was 0.47 dB for transmission over 1 span. Finally, the results presented in Fig.11 are also shown in terms of total throughput in Fig. 12.

Fig. 12 shows the total throughput achieved with each one of the amplification schemes by using Eq. (11). For transmission over a single span, the throughput values obtained are 319.72 Tbit/s, 310.72 Tbit/s, 296.48 Tbit/s, and 275.29 Tbit/s, respectively for the hybrid FW+BW-RA, hybrid BW-RA, hybrid FW-RA and LA. For the transmission after 10 spans, these values are respectively 213.16 Tbit/s, 204.51 Tbit/s, 189.9 Tbit/s, and 170.03 Tbit/s. Finally, for the transmission over 100 spans, these values are respectively 110.29 Tbit/s, 102.63 Tbit/s, 89.66 Tbit/s, and 74.34 Tbit/s.

IX. Conclusions

In this work, we presented the first ultra-wideband semi-analytical model to evaluate an optical fibre transmission system using hybrid amplification. This model is capable of accounting for any of Raman amplification configurations, namely, any number of pumps, forward and backward pumping regimes. It also accounts for the effect of inter-channel stimulated Raman scattering (ISRS), wavelength-dependent fibre parameters, different bandwidth per channel, any modulation format and arbitrary per-channel launch power values, including non-uniform launch power profiles. This model includes the estimation of fibre nonlinear interference and spontaneous emission noise generated by Raman and lumped amplified links. The TRX impairment can also be considered.

The model is an approximation in closed-form formula from the Gaussian noise model and was used in this paper for several analyses of hybrid amplified optical links, where distributed Raman amplification is used in combination with lumped amplifiers. It was demonstrated that the model is capable of accurately estimating the optical system performance after an arbitrary number of spans and is suitable for real-time estimation, optimisation routines and fast optical transmission performance analysis thanks to its speed of computation in the range of sub-seconds. Because of this, the formula can also be applied as an enabling tool for future intelligent and dynamic optical fibre networks.

The analysis in this work was carried out for an optical transmission system with 18.4 THz (145.7 nm) of optical signal, corresponding to the use of the S-, C- and L-bands. Scenarios ranging from short to metro, long-haul and trans-oceanic transmission systems were considered. For these scenarios, the best hybrid Raman amplifier was designed based on a particle swarm optimisation algorithm, where the optimised pump‘ wavelengths and powers were calculated to maximise the total system throughput of a multi-span system, with 80 km standard single-mode fibre spans. Launch power optimisation was also carried out to maximise the performance.

For the optimised hybrid amplifiers, their characterisation in terms of gain was presented. Moreover, all the sources of noise were analysed in detail, and their relation with the performance of the optical fibre amplifier technology chosen was also assessed. A comparison with an optimised fully lumped amplifier was presented showing how and why hybrid amplifiers can outperform EDFAs and TDFAs. This work also showed how to design high-capacity achieving hybrid amplifiers using analytical modelling.

Among the several new results of this paper, we described a hybrid forward + backward Raman amplifier achieving 319.82 Tbit/s over a single 80 km span transmission, a hybrid backward Raman amplifier achieving 310.72 Tbit/s, and a hybrid forward Raman amplifier achieving 296.48 Tbit/s, both over the same system. In comparison, a fully lumped optimised amplifier was shown to achieve no more than 275.29 Tbit/s under the same conditions. This represents throughput increases of 16.17 %, 12.87 % and 7.69 % respectively for optimised forward + backward, backward and forward hybrid Raman amplifiers compared to a fully lumped optimised amplifier.

Data Availability Statement

The data that support the figures in this paper are available from the UCL Research Data Repository (DOI:10.5522/04/25383073), hosted by FigShare.

References

[1] B. J. Puttnam, R. S. Luis, I. Phillips, M. Tan, A. Donodin, D. Pratiwi, L. Dallachiesa, Y. Huang, M. Mazur, N.K. Fontaine, H. Chen, D. Chung, V. Ho, D. Orsuti, B. Boriboon, G. Rademacher, L. Palmieri, R. Man, R. Ryf, D. T. Neilson, W. Forysiak, and H. Furukawa, “402 Tb/s GMI data-rate OESCLU-band transmission,” in *Optical Fiber Communication Conference (OFC) 2024*. 2024, p. Th4A.3, Optica Publishing Group.

[2] Benjamin J Puttnam, Ruben S Luís, Yetian Huang, Ian Phillips, Dicky Chung, Nicolas K Fontaine, Georg Rademacher, Mikael Mazur, Lauren Dallachiesa, Haoshuo Chen, Wladek Forysiak, Ray Man, Roland Ryf, David T Neilson, and Hideaki Furukawa, “301 Tb/s E, S, C+L-band transmission over 212 nm bandwidth with E-band Bismuth-doped fiber amplifier and gain equalizer,” in *2023 European Conference on Optical Communication (ECOC)*, 2023.

[3] Benjamin. J. Puttnam, Ruben. S. Luis, Yetian Huang, Ian Phillips, Dicky Chung, Nicolas K. Fontaine, Budsara Boriboon, Georg Rademacher, Mikael Mazur, Lauren Dallachiesa, Haoshuo Chen, Wladek Forysiak, Ray Man, Roland Ryf, David T. Neilson, and Hideaki Furukawa, “264.7 Tb/s E, S, C + L-band transmission over 200 km,” in *Optical Fiber Communication Conference (OFC) 2024*. 2024, p. M1F.4, Optica Publishing Group.

[4] Benjamin J. Puttnam, Ruben S. Luís, Georg Rademacher, Manuel Mendez-Astudillio, Yoshinari Awaji, and Hideaki Furukawa, "S-, C- and L-band transmission over a 157nm bandwidth using doped fiber and distributed Raman amplification," *Opt. Express*, vol. 30, no. 6, pp. 10011–10018, Mar 2022.

[5] Qingyu He, Dawei Ge, Ming Luo, Xu Zhang, Yan Wu, Liang Mei, Ping Du, Dong Wang, Hongguang Zhang, Han Li, and Xi Xiao, "150.27-Tb/s capacity over 150-km in S+C+L band using 156-channel 115-GBaud signals with doped fiber amplification," in *Optical Fiber Communication Conference (OFC) 2024*. 2024, p. Tu3E.2, Optica Publishing Group.

[6] Fukutaro Hamaoka, Masanori Nakamura, Minami Takahashi, Takayuki Kobayashi, Yutaka Miyamoto, and Yoshiaki Kisaka, "173.7-Tb/s triple-band WDM transmission using 124-channel 144-GBaud signals with SE of 9.33 b/s/Hz," in *2023 Optical Fiber Communications Conference and Exhibition (OFC)*. IEEE, 2023.

[7] Fukutaro Hamaoka, Masanori Nakamura, Takeo Sasai, Shuto Sugawara, Takayuki Kobayashi, Yutaka Miyamoto, and Etsushi Yamazaki, "110.7-Tb/s single-mode-fiber transmission over 1040 km with high-symbol-rate 144-GBaud PDM-PCS-QAM signals," in *Optical Fiber Communication Conference (OFC) 2024*. 2024, p. Tu3E.6, Optica Publishing Group.

[8] Benjamin J. Puttnam, Ruben S. Luís, Georg Rademacher, Manuel Mendez-Astudilio, Yoshinari Awaji, and Hideaki Furukawa, "S, C and extended L-band transmission with doped fiber and distributed Raman amplification," *Optical Fiber Communication Conference (OFC)*, p. Th4C.2, 2021.

[9] Lidia Galdino, Adrian Edwards, Wenting Yi, Eric Sillekens, Yuta Wakayama, Thomas Gerard, Wayne Sheldon Pelouch, Stuart Barnes, Takehiro Tsuritani, Robert I Killey, et al., "Optical fibre capacity optimisation via continuous bandwidth amplification and geometric shaping," *IEEE Photonics Technology Letters*, vol. 32, no. 17, pp. 1021–1024, 2020.

[10] Xiaohui Zhao and et. al, "200.5 Tb/s transmission with S+C+L amplification covering 150 nm bandwidth over 2×100 km PSCF spans," *2022 European Conference on Optical Communication (ECOC)*, p. Th3C.4, 2022.

[11] Jiaqian Yang, Romulo Aparecido, Henrique Buglia, Pratim Hazarika, Eric Sillekens, Ronit Sohanpal, Mingming Tan, Dini Pratiwi, Ruben S. Luis, Benjamin J. Puttnam, Yuta Wakayama, Wladek Forysiak, Polina Bayvel, and Robert I. Killey, "122.6-Tb/s S+C+L band unrepeated transmission over 223 km link with optimised bidirectional Raman amplication," in *2024 Optical Fiber Communications Conference and Exhibition (OFC)*. IEEE, 2023.

[12] Benjamin J. Puttnam, Ruben S. Luis, Georg Rademacher, Yoshinari Awaji, and Hideaki Furukawa, "Investigation of long-haul S-, C- + L-band transmission," in *2022 Optical Fiber Communications Conference and Exhibition (OFC)*, 2022.

[13] Fukutaro Hamaoka, Masanori Nakamura, Seiji Okamoto, Kyo Minoguchi, Takeo Sasai, Asuka Matsushita, Etsushi Yamazaki, and Yoshiaki Kisaka, "Ultra-wideband WDM transmission in S-, C-, and L-bands using signal power optimization scheme," *Journal of Lightwave Technology*, vol. 37, no. 8, pp. 1764–1771, 2019.

[14] J. Renaudier, A. Arnould, D. Le Gac, A. Ghazisaeidi, P. Brindel, M. Makhsiyan, A. Verdier, K. Mekhazni, F. Blache, H. Debregeas, A. Boutin, N. Fontaine, D. Neilson, R. Ryf, H. Chen, M. Achouche, and G. Charlet, "107 Tb/s transmission of 103-nm bandwidth over 3×100 km SSMF using ultra-wideband hybrid Raman/SOA repeaters," *Optical Fiber Communication Conference (OFC)*, p. Tu3F.2, 2019.

[15] J. Renaudier, A. C. Meseguer, A. Ghazisaeidi, P. Tran, R. R. Muller, R. Brenot, A. Verdier, F. Blache, K. Mekhazni, B. Duval, H. Debregeas, M. Achouche, A. Boutin, F. Morin, L. Letteron, N. Fontaine, Y. Frignac, and G. Charlet, "First 100-nm continuous-band WDM transmission system with 115Tb/s transport over 100km using novel ultra-wideband semiconductor optical amplifiers," in *European Conference on Optical Communication (ECOC)*, 2017.

[16] Amirhossein Ghazisaeidi, Aymeric Arnould, Maria Ionescu, Vahid Aref, Haik Mardoyan, Sophie Etienne, Mathieu Duval, Christian Bastide, Hans Bissessur, and Jeremie Renaudier, "99.35 Tb/s ultra-wideband unrepeated transmission over 257 km using semiconductor optical amplifiers and distributed Raman amplification," *Journal of Lightwave Technology*, vol. 40, no. 21, pp. 7014–7019, 2022.

[17] L. Galdino, D. Semrau, M. Ionescu, A. Edwards, W. Pelouch, S. Desbruslais, J. James, E. Sillekens, D. Lavery, S. Barnes, R. I. Killey, and P. Bayvel, "Study on the impact of nonlinearity and noise on the performance of high-capacity broadband hybrid Raman-EDFA amplified system," *Journal of Lightwave Technology*, vol. 37, no. 21, pp. 5507–5515, 2019.

[18] M. Ionescu, D. Lavery, A. Edwards, E. Sillekens, D. Semrau, L. Galdino, R. I. Killey, W. Pelouch, S. Barnes, and P. Bayvel, "74.38 Tb/s transmission over 6300 km single mode fibre enabled by C+L amplification and geometrically shaped PDM-64QAM," *Journal of Lightwave Technology*, vol. 38, no. 2, pp. 531–537, 2020.

[19] J. . Cai, H. G. Batshon, M. V. Mazurczyk, C. R. Davidson, O. V. Sinkin, D. Wang, M. Paskov, W. W. Patterson, M. A. Bolshtyansky, and D. G. Foursa, "94.9 Tb/s single mode capacity demonstration over 1,900 km with C+L EDFAs and coded modulation," in *European Conference on Optical Communication (ECOC)*, 2018.

[20] J. . Cai, H. G. Batshon, M. V. Mazurczyk, O. V. Sinkin, D. Wang, M. Paskov, W. Patterson, C. R. Davidson, P. Corbett, G. Wolter, T. Hammon, M. Bolshtyansky, D. Foursa, and A. Pilipetskii, "70.4 Tb/s capacity over 7,600 km in C+L band using coded modulation with hybrid constellation shaping and nonlinearity compensation," in *Optical Fiber Communications Conference (OFC)*, 2017.

[21] J. Cai, Y. Sun, H. Zhang, H. G. Batshon, M. V. Mazurczyk, O. V. Sinkin, D. G. Foursa, and A. Pilipetskii, "49.3 Tb/s transmission over 9100 km using C+L EDFA and 54 Tb/s transmission over 9150 km using hybrid-Raman EDFA," *Journal of Lightwave Technology*, vol. 33, no. 13, pp. 2724–2734, 2015.

[22] J. Cai, H. G. Batshon, M. V. Mazurczyk, O. V. Sinkin, D. Wang, M. Paskov, C. R. Davidson, W. W. Patterson, A. Turukhin, M. A. Bolshtyansky, and D. G. Foursa, "51.5 Tb/s capacity over 17,107 km in C+L bandwidth using single-mode fibers and nonlinearity compensation," *Journal of Lightwave Technology*, vol. 36, no. 11, pp. 2135–2141, 2018.

[23] Takeshi Hoshida, Vittorio Curri, Lidia Galdino, David T. Neilson, Wladek Forysiak, Johannes K. Fischer, Tomoyuki Kato, and Pierluigi Poggiolini, "Ultrawideband systems and networks: beyond C + L-band," *Proceedings of the IEEE*, vol. 110, no. 11, pp. 1725–1741, 2022.

[24] Henrique Buglia, Eric Sillekens, Anastasiia Vasylchenkova, Wenting Yi, Robert Killey, Polina Bayvel, and Lidia Galdino, "Challenges in extending optical fibre transmission bandwidth beyond C+L band and how to get there," in *2021 International Conference on Optical Network Design and Modeling (ONDM)*, 2021.

[25] H. Buglia, E. Sillekens, A. Vasylchenkova, P. Bayvel, and L. Galdino, "On the impact of launch power optimization and transceiver noise on the performance of ultra-wideband transmission systems [invited]," *Journal of Optical Communications and Networking*, vol. 14, no. 5, pp. B11–B21, 2022.

[26] Erik Agrell, Magnus Karlsson, Francesco Poletti, Shu Namiki, Xi (Vivian) Chen, Leslie A Rusch, Benjamin Puttnam, Polina Bayvel, Laurent Schmalen, Zhenning Tao, Frank R Kschischang, Alex Alvarado, Biswanath Mukherjee, Ramon Casellas, Xiang Zhou, Dora van Veen, Georg Mohs, Elaine Wong, Antonio Mecozzi, Mohamed-Slim Alouini, Eleni Diamanti, and Murat Uysal, "Roadmap on optical communications," *Journal of Optics*, vol. 26, no. 9, pp. 093001, jul 2024.

[27] André Souza, Nelson Costa, Jo ao Pedro, and Jo ao Pires, "Benefits of counterpropagating Raman amplification for multiband optical networks," *J. Opt. Commun. Netw.*, vol. 14, no. 7, pp. 562–571, Jul 2022.

[28] Pierluigi Poggiolini, "The GN model of non-linear propagation in uncompensated coherent optical systems," *Journal of Lightwave Technology*, vol. 30, no. 24, pp. 3857–3879, 2012.

[29] Andrea Carena, Gabriella Bosco, Vittorio Curri, Yanchao Jiang, Pierluigi Poggiolini, and Fabrizio Forghieri, "EGN model of non-linear fiber propagation," *Opt. Express*, vol. 22, no. 13, pp. 16335–16362, Jun 2014.

[30] Daniel Semrau, Robert I. Killey, and Polina Bayvel, "The Gaussian noise model in the presence of inter-channel stimulated Raman scattering," *Journal of Lightwave Technology*, vol. 36, no. 14, pp. 3046–3055, 2018.

[31] Nikita A. Shevchenko, Sam Nallaperuma, and Seb J. Savory, "Maximizing the information throughput of ultra-wideband fiber-optic communication systems," *Opt. Express*, vol. 30, no. 11, pp. 19320–19331, May 2022.

[32] Andrea D'Amico, Bruno Correia, Elliot London, Emanuele Virgillito, Giacomo Borraccini, Antonio Napoli, and Vittorio Curri, "Scalable and disaggregated GGN approximation applied to a C+L+S optical network," *Journal of Lightwave Technology*, vol. 40, no. 11, pp. 3499–3511, 2022.

[33] Mindaugas Jarmolovičius, Daniel Semrau, Henrique Buglia, Mykyta Shevchenko, Filipe M. Ferreira, Eric Sillekens, Polina Bayvel, and Robert I. Killey, "Optimising O-to-U band transmission using fast ISRS Gaussian noise numerical integral model," *arXiv:2401.18022 [eess.SP]*, 2024.

[34] Gabriella Bosco, "Complexity versus accuracy tradeoffs in nonlinear fiber propagation models," *Optical Fiber Conference (OFC)*, 2023.

[35] P. Poggiolini, M. Ranjbar Zefreh, G. Bosco, F. Forghieri, and S. Piciaccia, "Accurate non-linearity fully-closed-form formula based on

the GN/EGN model and large-data-set fitting," in *2019 Optical Fiber Communications Conference and Exhibition (OFC)*, 2019.

[36] Daniel Semrau, Robert I. Killey, and Polina Bayvel, "A closed-form approximation of the Gaussian noise model in the presence of inter-channel stimulated Raman scattering," *Journal of Lightwave Technology*, vol. 37, no. 9, pp. 1924–1936, 2019.

[37] Mahdi Ranjbar Zefreh, Fabrizio Forghieri, Stefano Piciaccia, and Pierluigi Poggiolini, "Accurate closed-form real-time EGN model formula leveraging machine-learning over 8500 thoroughly randomized full C-band systems," *Journal of Lightwave Technology*, vol. 38, no. 18, pp. 4987–4999, 2020.

[38] Daniel Semrau, Eric Sillekens, Robert I. Killey, and Polina Bayvel, "A modulation format correction formula for the Gaussian noise model in the presence of inter-channel stimulated Raman scattering," *Journal of Lightwave Technology*, vol. 37, no. 19, pp. 5122–5131, 2019.

[39] Mahdi Ranjbar Zefreh and Pierluigi Poggiolini, "A real-time closed-form model for nonlinearity modeling in ultra-wide-band optical fiber links accounting for inter-channel stimulated Raman scattering and co-propagating Raman amplification," *arXiv:2006.03088 [eess.SP]*, 2020.

[40] M. Ranjbar Zefreh, F. Forghieri, S. Piciaccia, and P. Poggiolini, "A closed-form nonlinearity model for forward-Raman-amplified WDM optical links," in *Optical Fiber Communication Conference (OFC) 2021*. 2021, p. M5C.1, Optica Publishing Group.

[41] Pierluigi Poggiolini and Mahdi Ranjbar-Zefreh, "Closed form expressions of the nonlinear interference for UWB systems," in *2022 European Conference on Optical Communication (ECOC)*, 2022.

[42] H. Buglia, E. Sillekens, A. Vasylchenkova, R.I. Killey, P. Bayvel, and L. Galdino, "An extended version of the ISRS GN model in closed-form accounting for short span lengths and low losses," in *2022 European Conference on Optical Communication (ECOC)*, 2022.

[43] H. Buglia, M. Jarmolovičius, A. Vasylchenkova, E. Sillekens, L. Galdino, R. I. Killey, and P. Bayvel, "A closed-form expression for the Gaussian noise model in the presence of inter-channel stimulated Raman scattering extended for arbitrary loss and fibre length," *Journal of Lightwave Technology*, pp. 1–10, 2023.

[44] Daniel Semrau, Gabriel Saavedra, Domaniç Lavery, Robert I. Killey, and Polina Bayvel, "A closed-form expression to evaluate nonlinear interference in Raman-amplified links," *Journal of Lightwave Technology*, vol. 35, no. 19, pp. 4316–4328, 2017.

[45] Henrique Buglia, Mindaugas Jarmolovicius, Anastasiia Vasylchenkova, Eric Sillekens, Lidia Galdino, Polina Bayvel, and Robert Killey, "A closed-form expression for the ISRS GN model supporting distributed Raman amplification," *Optical Fiber Conference (OFC)*, 2023.

[46] Henrique Buglia, Mindaugas Jarmolovičius, Lidia Galdino, Robert I. Killey, and Polina Bayvel, "A closed-form expression for the gaussian noise model in the presence of Raman amplification," *Journal of Lightwave Technology*, vol. 42, no. 2, pp. 636–648, 2024.

[47] H. Buglia, M. Jarmolovicius, L. Galdino, R. I. Killey, and P. Bayvel, "A modulation-format dependent closed-form expression for the Gaussian noise model in the presence of Raman amplification," *European Conference on Optical Communication (ECOC)*, 2023.

[48] Henrique Buglia, Eric Sillekens, Lidia Galdino, Robert Killey, and Polina Bayvel, "Throughput maximisation in ultra-wideband hybrid-amplified links," in *Optical Fiber Communication Conference (OFC) 2024*. 2024, p. Tu3H.5, Optica Publishing Group.

[49] Yanchao Jiang and Pierluigi Poggiolini, "CFM6, a closed-form NLI EGN model supporting multiband transmission with arbitrary Raman amplification," *arXiv:2405.08512 [eess.SP]*, 2024.

[50] Ian Roberts, Joseph M Kahn, James Harley, and David W Boertjes, "Channel power optimization of WDM systems following Gaussian noise nonlinearity model in presence of stimulated Raman scattering," *Journal of Lightwave Technology*, vol. 35, no. 23, pp. 5237–5249, 2017.

[51] Sam Nallaperuma, Nikita A. Shevchenko, and Seb J. Savory, "Parameter optimisation for ultra-wideband optical networks in the presence of stimulated Raman scattering effect," in *International Conference on Optical Network Design and Modeling (ONDM)*, 2021.

[52] Bruno Correia, Rasoul Sadeghi, Emanuele Virgillito, Antonio Napoli, Nelson Costa, João Pedro, and Vittorio Curri, "Optical power control strategies for optimized C+L+S-bands network performance," in *Optical Fiber Communications Conference*, 2021.

[53] A. M. Rosa Brusin, M. Ranjbar Zefreh, P. Poggiolini, S. Piciaccia, F. Forghieri, and A. Carena, "Machine learning for power profiles prediction in presence of inter-channel stimulated Raman scattering," in *European Conference on Optical Communication (ECOC)*, 2021.

[54] Bruno Correia, Rasoul Sadeghi, Emanuele Virgillito, Antonio Napoli, Nelson Costa, Joao Pedro, and Vittorio Curri, "Power control strategies and network performance assessment for C+L+S multiband optical transport," *Journal of Optical Communications and Networking*, vol. 13, no. 7, pp. 147–157, 2021.

[55] Daniel Semrau, Robert I. Killey, and Polina Bayvel, "A closed-form approximation of the Gaussian noise model in the presence of inter-channel stimulated Raman scattering," *Journal of Lightwave Technology*, vol. 37, no. 9, pp. 1924–1936, 2019.

[56] Pierluigi Poggiolini, "A generalized GN-model closed-form formula.," *arXiv:1810.06545 [eess.SP]*, 2018.

[57] Uiara C. de Moura, Francesco Da Ros, A. Margareth Rosa Brusin, Andrea Carena, and Darko Zibar, "Experimental characterization of Raman amplifier optimization through inverse system design," *Journal of Lightwave Technology*, vol. 39, no. 4, pp. 1162–1170, 2021.

[58] M Soltani, F Da Ros, A Carena, and D Zibar, "Distance and spectral power profile shaping using machine learning enabled Raman amplifiers," in *IEEE Photonics Society Summer Topicals Meeting Series (SUM)*, 2021.

[59] Viacheslav V. Ivanov, Lidia Galdino, and John D. Downie, "Optimization of channel powers, Raman pumps and EDFAs in the wideband fiber optic transmission systems," in *Optical Fiber Communication Conference (OFC) 2024*. 2024, p. W2B.1, Optica Publishing Group.

[60] Henrique Buglia, Eric Sillekens, Lidia Galdino, Robert I. Killey, and Polina Bayvel, "Impact of launch power optimisation in hybrid-amplified links," *arXiv:2405.17443 [eess.SP]*, 2024.

[61] Yanchao Jiang, Antonino Nespola, Alberto Tanzi, Stefano Piciaccia, Mahdi Ranjbar Zefreh, Fabrizio Forghieri, and Pierluigi Poggiolini, "Performance enhancement of long-haul C+L+S systems by means of CFM-assisted optimization," in *Optical Fiber Communication Conference (OFC) 2024*. 2024, p. M1F.2, Optica Publishing Group.

[62] Jake Bromage, "Raman amplification for fiber communications systems," *J. Lightwave Technol.*, vol. 22, no. 1, pp. 79, Jan 2004.

[63] Md Asif Iqbal, Gabriele Di Rosa, Lukasz Krzczanowicz, Ian Phillips, Paul Harper, André Richter, and Wladek Forysiak, "Impact of pump-signal overlap in S+C+L band discrete Raman amplifiers," *Opt. Express*, vol. 28, no. 12, pp. 18440–18448, Jun 2020.

[64] J. Kennedy and R. Eberhart, "Particle swarm optimization," *Proceedings of ICNN'95 - International Conference on Neural Networks*, vol. 4, pp. 1942–1948, 1995.

[65] C.R. Giles and E. Desurvire, "Propagation of signal and noise in concatenated erbium-doped fiber optical amplifiers," *Journal of Lightwave Technology*, vol. 9, no. 2, pp. 147–154, 1991.

[66] Alberto Bononi, Jean-Christophe Antona, Paolo Serena, Alexis Carbo-Meseguer, and Chiara Lasagni, "The generalized droop model for submarine fiber-optic systems," *Journal of Lightwave Technology*, vol. 39, no. 16, pp. 5248–5257, 2021.

[67] Alberto Bononi, Jean-Christophe Antona, Paolo Serena, Alexis Carbo-Meseguer, and Chiara Lasagni, "The generalized droop model for submarine fiber-optic systems," *Journal of Lightwave Technology*, vol. 39, no. 16, pp. 5248–5257, 2021.